Paleoceanography and Paleoclimatology

RESEARCH ARTICLE
10.1029/2020PA003958

Reconstructing Western Boundary Current Stability in the North Atlantic Ocean for the Past 700 Kyr From *Globorotalia truncatulinoides* Coiling Ratios

Katharina Billups[1], Maoli Vizcaíno[1], Josephine Chiarello[1,2], and Emily A. Kaiser[1,3]

[1]School of Marine Science and Policy, University of Delaware, Lewes, DE, USA, [2]Department of Geology, University of Cincinnati, Cincinnati, OH, USA, [3]Now at College of Marine Science, University of South Florida, St. Petersburg, FL, USA

Key Points:
- Consistent coupling between *G. truncatulinoides* coiling ratios, total test counts, and bulk sediment $CaCO_3$ content begins with MIS 11
- Sinistral maxima during MIS 7a, 5c–5e, 1, and minima during MIS 11c, 9c–9e, occur with high test counts reflecting intensified circulation
- Sinistral maxima (MIS 5c–5e, 1) and minima (MIS 11c, 9c–9e) are prolonged indicating stability of the boundary current during warm intervals

Correspondence to:
K. Billups,
kbillups@udel.edu

Citation:
Billups, K., Vizcaíno, M., Chiarello, J., & Kaiser, E. A. (2020). Reconstructing western boundary current stability in the North Atlantic Ocean for the past 700 kyr from *Globorotalia truncatulinoides* coiling ratios. *Paleoceanography and Paleoclimatology*, *35*, e2020PA003958. https://doi.org/10.1029/2020PA003958

Received 19 APR 2020
Accepted 1 NOV 2020
Accepted article online 16 NOV 2020

Abstract Down-core changes in the coiling direction of *Globorotalia truncatulinoides* in the northwestern subtropical Atlantic (KNR140-37PC and Ocean Drilling Program Sites 1063, 1059, 1056, 1058) provide a tracer for the hydrographic conditions in the western boundary current over the past 700 kyr (Marine Isotope Stage, MIS, 1–17). A consistent association between percent *G. truncatulinoides* (sinistral) abundances, total test counts, and bulk sediment $CaCO_3$ content is established by MIS 11 suggesting a response to ocean-atmosphere interactions during the mid Brunhes event. Commencing with MIS 11, interglacial maxima are associated with high total test counts and either distinct sinistral test minima (MIS 9e, 11c) or maxima (MIS 1, 5e, 7a). High sinistral test abundances with relatively high test counts is similar to the late Holocene relationship at the study sites. Low sinistral test abundances despite high test counts means that coiling ratios are dominated by dextral forms. We interpret this pattern to indicate more intense flow in the subtropical gyre either via the western boundary current drawing toward the gyre center, or a more northern influence of the North Equatorial and Antilles Currents. This suggests that the western boundary current may have been more intense during MIS 11c and MIS 9e then during MIS 7a, MIS 5e, and MIS 1 consistent with climate warm anomalies in northern Europe at these times. Regardless of the mechanism, the observation that minima and maxima in sinistral test abundances are prolonged at these times indicates that the western gyre boundary remained stable during relative warm intervals.

1. Introduction

Understanding the relative stability of the subtropical gyre during climatic warm intervals has important implications for assessing the potential magnitude of sea level rise along continental margins. A case in point, a recent increase in sea level along the U.S. mid-Atlantic coast of up to 3 to 4 times the glacioeustatic rise can be attributed to a weakening of the Gulf Stream system (Ezer et al., 2013; Sallenger et al., 2012). In this vein, enhanced gyre flow would mitigate some of the glacioeustatic sea level rise in this region by drawing the warm current away from the coast. On a more global scale, variations in Gulf Stream flow, and its extension the North Atlantic Current, also affect ocean-atmosphere interactions in the North Atlantic and therefore deepwater formation rates and meridional overturning circulation (Rahmstorf, 2002; Sallenger et al., 2012).

On glacial-to interglacial time scales, however, it is not clear whether or not the overall position of the Gulf Stream varies. For the Last Glacial Maximum (LGM), planktic foraminiferal (*Globorotalia truncatulinoides*) $\delta^{18}O$ values do not provide evidence for a shift in the latitude of separation of the current from the continent (LeGrande & Lynch-Stieglitz, 2007; Matsumoto & Lynch-Stieglitz, 2003). The intensity of the flow, on the other hand, may have been reduced by 30–50% (Lynch-Stieglitz et al., 1999). Planktic $\delta^{18}O$ values and faunal assemblages from the LGM suggest that the subtropical gyre was more compressed implying a change in the latitude of the Gulf Stream system after it leaves the coast (Billups & Schrag, 2000; Pflaumann et al., 2003). Changes in *G. truncatulinoides* coiling direction, a proxy for the relative depth of the permanent thermocline in the North Atlantic (e.g., Feldmeijer et al., 2014), support a change in the western boundary current of the subtropical gyre during the last two glacial cycles (Marine Isotope Stages, MIS, 6–1) (Billups et al., 2016).

Here we use down-core variations in the *G. truncatulinoides* coiling direction to reconstruct the relative stability of the northwestern boundary current of the North Atlantic subtropical gyre over the past 700 kyr (MIS 1–17). Our study extends the results from Billups et al. (2016), who demonstrate that

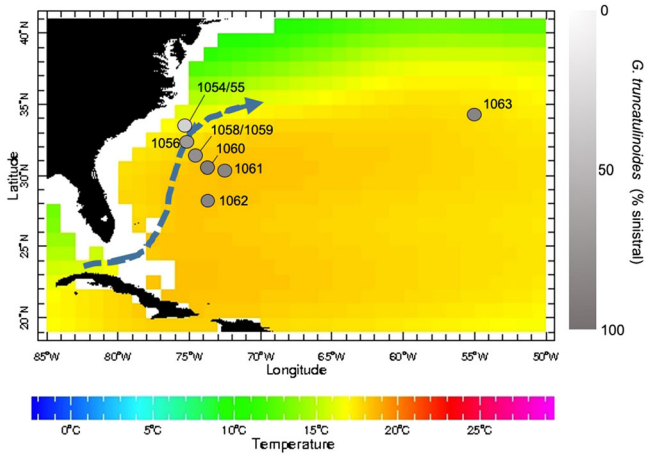

Figure 1. Ocean Drilling Program Leg 172 Sites 1054–1062 on the Carolina slope and Blake Bahama outer ridge and Site 1063 from Bermuda rise (circles). Sites 1056, 1058, 1059, and 1063 are the focus of down-core reconstructions. Color reflects water temperature at 300-m water depth (WOA09, Locarnini et al., 2010), the depth of maximum *Globorotalia truncatulinoides* abundances in this region (Ujiié et al., 2010). Gray shading of the site location symbols indicates the percentage of *G. truncatulinoides* (sinistral) in core top sediments (Kucera et al., 2005) (Table 1), some of which have been averaged here for clarity. The dashed arrow shows the approximate position of the Gulf Stream along the western margin of the gyre (after Matsumoto & Lynch-Stieglitz, 2003). The figure was generated using the interactive website from the LDEO.

prolonged maxima in sinistral tests at Blake Bahama Outer Ridge (BBOR) reflect enhanced subtropical gyre flow during interglacial MIS 1 and MIS 5 in comparison to glacial MIS 2–4 and MIS 6. In this study, we use an array of sites (Figure 1) so that at least two sites record a similar temporal interval and thus duplicate the observations for a more confident reconstruction of gyre dynamics through time. The temporal resolution (e.g., 0.5–2 kyr time step) resolves orbital signals as well as higher-frequency variability within the overall glacial and interglacial climate context.

Specifically, the five study sites (KNR140-37PC and Ocean Drilling Program, ODP, Sites 1063, 1059, 1056, and 1058) span the Holocene through the mid-Pleistocene (~0–700 ka, MIS 1–17) (Table 1). The most recent interval is represented by gyre center Site 1063, which extends from the Holocene to ~280 ka (MIS 1–8) paralleling published data from gyre margin core KNR140-37PC (Billups et al., 2016) until 134 ka. Site 1059, for which the MIS 6–8 (134–271 ka) portion was also published by Billups et al. (2016), extends the gyre margin record to 412 ka (MIS 11). Between 240 and 400 ka (MIS 8 through MIS 11), the record overlaps with the one from Site 1056, and because they are within 1° latitude/longitude, provide a duplication of results. Site 1056 then extends through 435 ka (MIS 12) and connects with the record from Site 1058 (Kaiser et al., 2019). As our focus is on the later Pleistocene, we only show the 411–700 ka (MIS 11–17) portion of this record, which we have augmented with new data points to increase the temporal resolution to that of the other sites (0.5–2 kyr).

2. *Globorotalia truncatulinoides* as a Paleoceanographic Proxy (a Brief Review)

Originally, *G. truncatulinoides* were used as index fossils marking the beginning of the Pleistocene denoting glacial versus interglacial stages (e.g., Hemleben et al., 1985). Early studies of *G. truncatulinoides* used morphological characteristics to classify different types until molecular data and genetic species concepts led to a refined understanding of *G. truncatunlinoides* biodiversity and phylogeny (De Vargas et al., 2001). Molecular studies indicate that the species has five genetically distinct types (types I–V) associated with different geographical locations spanning the world oceans (De Vargas et al., 2001; Quillévéré et al., 2013; Ujiié & Lipps, 2009; Ujiié et al., 2010).

In the North Atlantic, our study region, only type II occurs (e.g., Ujiié et al., 2010, and references therein). Type II exhibits two coiling directions, sinistral and dextral. Molecular clocks indicate that this type may have split from its ancestor, type I, a sinistral form, as recently as 170 kyr ago (De Vargas et al., 2001). Down-core studies in the western subtropical Atlantic Ocean, however, have distinguished dextral from sinistral tests during the middle Pleistocene (Chaisson et al., 2002; Kaiser et al., 2019) suggesting that branching occurred earlier. The relative abundance of sinistral versus dextral tests in type II *G. truncatulinoides* was recognized in early paleocenographic studies as linked to specific water masses and environmental parameters (e.g., Ericson et al., 1954; Herman, 1972; Thiede, 1971). Plankton tows confirm inferences from core top sediments used in these early studies. In such tows, the left coiling variety, *G. truncatulinoides* (sinistral), dominates regions characterized by a relatively homogenous upper water column with a deep permanent thermocline such as the center of the subtropical gyre of the North Atlantic (Ujiié et al., 2010). There, during the winter months phytoplankton blooms and the chlorophyll maximum is deep (Deuser & Ross, 1989). *G. truncaulinoides* (dextral) are more abundant toward the southern extent of the gyre where the water column is stratified and nutrients are advected with the North Equatorial Current (Ujiié et al., 2010). This link between dominant coiling direction and water column structure has recently been explored as a proxy for temporal changes in upper ocean hydrography in the North Atlantic Ocean on geologic time scales (Billups et al., 2016; Feldmeijer et al., 2014; Kaiser et al., 2019).

Table 1
Site Location Summary Including the Relative Abundance of Globorotalia truncatulinoides (Sinistral) in Core Tops of the Northwestern Subtropical Atlantic Ocean

Site	Latitude (°N)	Longitude (°W)	Water depth (m)	MIS	Core top (%)	Age model source[a]
1054[b]	33.0	76.28	1,293	1	36	
1055[b]	32.78	76.29	1,798	1	35	
1056[b]	32.49	76.33	2,166	8–12	67	a
1057[b]	32.03	76.08	2,485	1	50	
1058[b,c]	31.69	75.43	2,984	11–16	78	b
1059[b]	31.69	75.42	2,996	5e–11[d]	78	c
1060[b]	30.76	74.47	3,481	1	86	
1061	29.98	73.60	4,038	1	82	
1062[b]	28.25	74.47	4,760	1	81	
1063[e]	33.67	57.62	4,583	1–6	83	d
KNR140-37PC	31.68	75.42	3,000	1–5	78	e

[a]a = oxygen isotope stratigraphy of Billups et al. (2004, 2011), b = oxygen isotope stratigraphy of Weirauch et al. (2008), c = MIS 5e-8: Oxygen isotope stratigraphy of Billups and Scheinwald (2014), MIS 9–11 ages are tuned to Site 1056 via the two sites' $CaCO_3$ records (Grützner et al., 2002); d = oxygen isotope stratigraphy of Channell et al. (2012) with revisions in 2016 (J. E. T. Channell, personal communication, 2020), e = oxygen isotope stratigraphy of Hagen and Keigwin (2002) with revision by Billups et al. (2016). [b]Data from Kucera et al. (2005). [c]Lower resolution down-core data set is from Kaiser et al. (2019). [d]Data for MIS 6–8 are from Billups et al. (2016). [e]Core top data are from his study.

3. Site Location and Proof of Concept

Study sites were drilled on BBOR (Sites 1056, 1058, and 1059) and Bermuda Rise (Site 1063) during ODP Leg 172 (Table 1, Figure 1). Sites 1056–1059 underlie the northwestern margin of the subtropical gyre underneath its northwestern boundary, the Gulf Stream, while Site 1063 lies in the center of the gyre. The upper water column at all sites is characterized by the presence of a deep permanent thermocline between 600–800 m water depth (Figure 2). The deep permanent thermocline with an overlying seasonally unstratified water column provides ideal conditions for *G. truncatulinoides* (sinistral) in the modern ocean.

At the study sites, core top percent *G. truncatulinoides* (sinistral) (defined as sinistral *G. truncatulinoides* counts/total *G. truncatulinoides* counts × 100) change across the northwestern gyre margin (Figure 1,

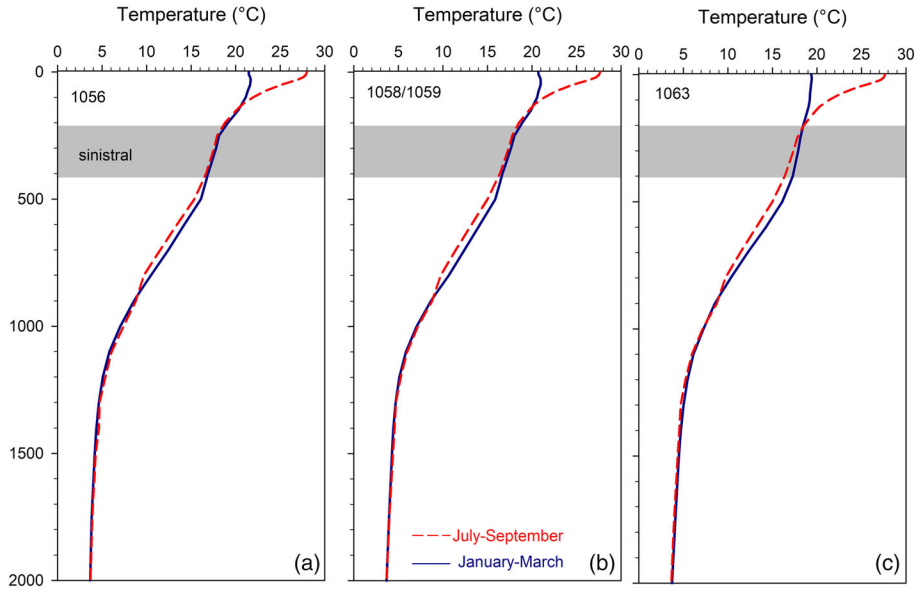

Figure 2. Vertical water column temperature profiles at the study sites (a) 1056, (b) 1058/1059, and (c) 1063 (solid blue line corresponds to January–March and dashed red line corresponds to July–September). At all sites the permanent thermocline is deep, and the water column is less stratified during the winter months. The gray bar indicates the depth at which *Globorotalia truncatulinoides* (sinistral) are most abundant according to plankton tows from this general area (Ujiié et al., 2010).

Table 1). Sites 1054 and 1055, although not part of the down-core study presented here, lie shoreward of the Gulf Stream outside the deep subtropical warm pool as defined by the 18°C isotherm at around 300 m water depth (Figure 1). At these two sites *G. truncatulinoide*s (sinistral) are in the minority (36% and 35%, respectively). Sites 1056 and 1057 lie closer to the axis of the Gulf Stream, and core top sediments contain a higher number of sinistral tests (67% and 50%, respectively). Sites 1058 and 1059 lie to the southeast of Sites 1056/1057, gyreward of the Gulf Stream, within the deep subtropical warm pool. Core top sediments are dominated by the left-coiling variety (78%). The location of Site 1059 is essentially the same as piston core KNR140-37PC where core top abundances are 75% (Billups et al., 2016). Sites 1060–1062 lie to the southeast of the study sites, and, at 81–86%, have the highest abundances of *G. truncatulinoides* (sinistral). Bermuda Rise Site 1063 lies near the center of the subtropical gyre, and, as at western margin Sites 1060–1062, *G. truncatulinoides* (sinistral) dominate core top sediments (83%). Thus, the close-up shown in Figure 1 illustrates how the dominant coiling direction of *G. truncatulinoides* increases across the Gulf Stream toward the center of the gyre.

4. Age Model

The age models of the study sites are based on published oxygen isotope stratigraphies (Table 1, Figure 3). Comparison of the Lisiecki and Raymo (2005) global benthic foraminiferal $\delta^{18}O$ stack (LR04) (Figure 3a) with the individual $\delta^{18}O$ records from each site indicates excellent agreement on the scale of individual MIS and their substages (Figure 3b). There is one exception, at Site 1058, MIS 13a is about ~17 kyr too young. In addition, the $\delta^{18}O$ minimum at 290 ka, which lies within MIS 8 (Figure 3a), provides an exception to the LR04 scheme. It has recently been reassigned as MIS 9a (Railsback et al., 2015). As illustrated in Figure 3, we follow the substage lettering of Railsback et al. (2015) throughout this study visually grouping this substage with interglacial MIS 9.

The MIS 9–11 portion of Site 1059 does not have a corresponding $\delta^{18}O$ record. To bring the age model into alignment with the other records, we adjusted the site's percent $CaCO_3$ record to the percent $CaCO_3$ record of Site 1056 (Grützner et al., 2002), the ages of which we have revised here on the basis of the site's published oxygen isotope stratigraphy (Billups et al., 2011).

5. Methods

All bulk sediment samples for this study have been previously processed in the context of other studies (Site 1063: Channell et al., 2012; Site 1059: Billups & Scheinwald, 2014; Site 1056: Billups et al., 2004, 2011; Site 1058: Weirauch et al., 2008) (Table 1). From the thus available coarse fractions, *G. truncatulinoides* coiling ratios were counted in core intervals to obtain an average time step of 0.5–2 kyr.

At Sites 1056–1059 *G. truncatulinoides* coiling ratios were determined from the 355–500 μm size fraction, and at Site 1063, we picked from the >250 μm fraction because abundances were generally lower. As suggested by Feldmeijer et al. (2014), and also shown by Kaiser et al. (2019), the different size fractions are comparable. Sample intervals were split until 100 tests could be counted. In intervals with low abundances, such as from glacial intervals, the entire sample was counted. To avoid noise introduced by calculating percentages from low counts, we only show data from intervals where at least 20 tests could be counted. We deem counts >20 robust given that we are only concerned with two coiling directions. This results in 8%, 19%, and 30% missing values at Sites 1056, 1059, and 1058 respectively. At Site 1063, which is deep (4,583 m), about half of the intervals had fewer than 20 total tests.

We recognize the potential bias introduced by low and variable overall *G. truncatulinoides* counts and therefore consider the total number of tests per sample interval (calculated from the split fraction). At each site sampling reflects the same amount of bulk sediment (10 ccs except at Site 1063, where 20 ccs were sampled, Channell et al., 2012), or a dry weight of about 13 ± 3 g on average. Therefore, the total counts at each particular site are not an artifact of variable sample size.

Additionally, we compare the total *G. truncatulinoides* counts to the published percent $CaCO_3$ records of the sites (Grützner et al., 2002). At BBOR and Bermuda Rise orbital-scale changes in the percent $CaCO_3$ reflect dilution with terrigenous sediments deposited by bottom water currents and dissolution due to bottom water mass chemistry (Grützner et al., 2002; Keigwin et al., 1998). These studies show that both effects increase

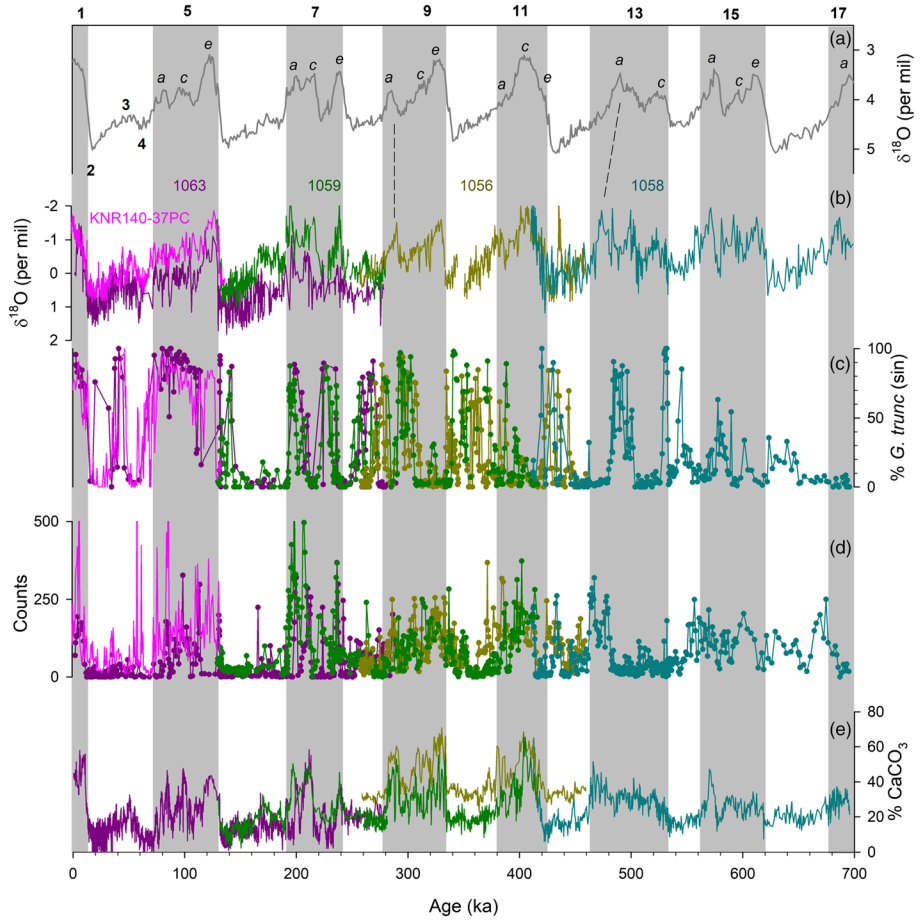

Figure 3. Comparison of the global benthic foraminiferal $\delta^{18}O$ stack (Lisiecki & Raymo, 2005) (a) to the individual planktic foraminiferal $\delta^{18}O$ records from each site (Table 1) (b), percent *Globorotalia truncatulinoides* (sinistral) (c), total *G. truncatulinoides* test counts (d), and percent $CaCO_3$ (e). The gray bars highlight odd-numbered marine isotope stages (labeled across the top) with stage boundaries according to Lisiecki and Raymo (2005) and substage lettering after Railsback et al. (2015). Dashed lines point toward deviations from the general MIS numbering scheme based on the $\delta^{18}O$ stack during MIS 9, and an age model discrepancy during MIS 13a.

with water depth and are more extreme during glacial intervals. Thus, comparison to the $CaCO_3$ record provides a measure of the degree to which variations in *G. truncatulinoides* total counts are affected by changes in the depositional environment. Neither dilution nor dissolution, however, bias the *G. truncatulinoides* coiling ratios.

6. Results

Compiling the individual records affords a first-order look at the relationship between the proxies over the past seven glacial to interglacial cycles (Figure 3). The composite illustrates that, overall, variations in the *G. truncatulinoides* (sinistral) abundances are not strictly tied to glacial–interglacial climate change as outlined by the $\delta^{18}O$ records (Figure 3c). Between MIS 17a and MIS 13a, sinistral test abundances increase from near 0% to a distinct maximum of ~100%. From MIS 12 through MIS 7, percentages vary with maxima of >70% and minima of <20% during both glacial and interglacial intervals. After MIS 7, maxima occur consistently during interglacial intervals (MIS 5e and MIS 1) and minima during glacial intervals (MIS 6, 4, and 2). MIS 3 provides an exception to the pattern with distinct maxima during a relatively cold stage. The new data from gyre center Site 1063 parallel the results from the gyre margin piston core and Site 1059.

Variations in total *G. truncatulinoides* test counts largely parallel those of the percent $CaCO_3$ record (Figures 3d and 3e, respectively). Both records display a first pronounced maximum during the end of MIS 13 (MIS 13a). Test counts are variable during MIS 12 when $CaCO_3$ is low. Beginning with MIS 11,

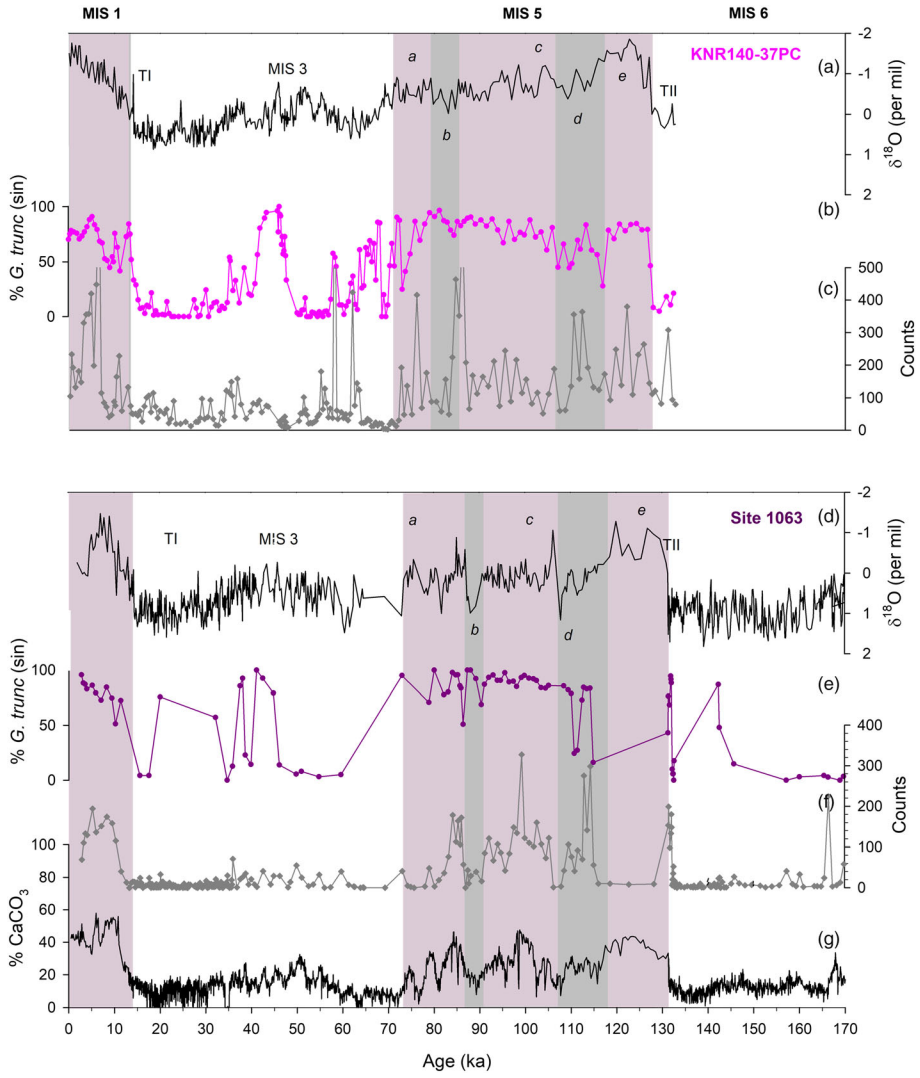

Figure 4. Results from piston core KNR140-37PC (top panel) and Ocean Drilling Program Site 1063 (bottom panel). Shown are (a and d) the sites' planktic (*Globigerinoides ruber*) foraminiferal $\delta^{18}O$ records (Table 1), (b and e) percent *Globorotalia truncatulinoides* (sinistral), (c and f) total *G. truncatulinoides* test counts, and (g) percent $CaCO_3$ (Site 1063 only, Grützner et al., 2002). Marine isotope stages (MIS) are labeled across the top. The color/gray bars identify the marine isotope substages with lettering after Railsback et al. (2015).

a distinct glacial to interglacial pattern becomes established with high counts and high percent $CaCO_3$ during odd MIS reflecting general interglacial intervals versus low counts and low percent $CaCO_3$ during even MIS defining overall glacial climates. Below we provide a more detailed look at the relationship between variations in the coiling direction and total test abundances with a focus on interglacial intervals.

6.1. MIS 1–6 (KNR140-37PC, Site 1063)

MIS 1–6 are recorded at gyre margin piston KNR140-37PC and gyre center Site 1063 (Figure 4, top and bottom panels, respectively). The planktic foraminiferal $\delta^{18}O$ record (*Globigerinoides ruber*) from both sites outlines the last (MIS 2–1) and penultimate (MIS 6–5) glacial to interglacial transitions Termination (T) TI and TII, respectively (Figures 4a and 4d), with only small (<4 kyr) age model discrepancies. Individual $\delta^{18}O$ minima and maxima during MIS 5 can be resolved in both records and assigned to substages MIS 5a–5e.

Results from KNR140-37PC have been discussed previously by Billups et al. (2016). Briefly, *G. truncatulinoides* (sinistral) percentages increase rapidly during TII and TI and remain high (>80%) during the

ensuing interglacial intervals (Figure 4b). Substage MIS 5d displays minor minima, and percentages decrease in a stepwise fashion during MIS 5a. Except for a distinct maximum during MIS 3 (>70%), sinistral abundances are low (<10%) during the generally glacial conditions spanning MIS 2–4. Thus, the coiling direction record varies between maxima and minima with few intermediate data points.

Total counts, on the other hand, are more variable at this gyre margin site. Counts are relatively high during MIS 5, decrease during MIS 5a, remain low during the entire MIS 2–4 interval, and increase again during the deglaciation when percent sinistral test abundances increase again (Figure 4c).

With the exception of TII and MIS 5e, gyre center Site 1063 *G. truncatulinoides* (sinistral) show similar trends with a prolonged maximum (>70%) during the majority of MIS 5a–5d, a rapid increase during TI, and a maximum during MIS 1. Minima (<10%) occur during glacial intervals MIS 6, 4, and 2 (Figure 4e). At this site, too, there is a distinct sinistral test maximum during MIS 3 despite low counts. And, the coiling direction record varies from maxima >70% to minima near 0% with few intermediate data points.

Total counts are lower than at the gyre margin site. There are frequent minima to <20 tests during glacial MIS 2–4, MIS 6, and interglacial MIS 5e (Figure 5f) resulting in relatively large gaps in the percent sinistral record (Figure 4e).

At this site, glacial MIS 2, 4, and 6 are also times of minimal $CaCO_3$ content (<20%) (Figure 4g). *G. truncatulinoides* are only present in significant numbers (i.e., >20, Figure 4f) when percent $CaCO_3$ is > ~ 20% (Figure 4g). Extremely low abundances (<10) of *G. truncatulinoides* during the interglacial MIS 5e, however, are not consistent with low glacial carbonate content. Percent $CaCO_3$ is high at this time, and the perceived lack of *G. truncatulinoides* in the gyre center must be due to an increase in the relative abundance of other carbonate producers.

6.2. MIS 7 (Sites 1063 and 1059)

MIS 7 and the shouldering parts of MIS 6 and 8 are recorded at gyre center Site 1063 and gyre margin Site 1059 (Figure 5, top and bottom panels, respectively). The *G. ruber* $\delta^{18}O$ record from Site 1063 does not show a pronounced transition between glacial MIS 8 and interglacial MIS 7 (TIII) or distinct variations related to climatic changes recorded by the marine isotope substages (Figure 5a). However, because $\delta^{18}O$ minima relate to $CaCO_3$ maxima and vice versa (Grützner et al., 2002), the $CaCO_3$ record aids in the identification of MIS 7a–7e (Figure 5d). At Site 1059, TIII as well as MIS 7a–7e are well defined in the *G. ruber* $\delta^{18}O$ (Figure 5e).

At both sites, the percentage of *G. truncatulinoides* (sinistral) is variable, and it is difficult to discern a consistent common pattern (Figure 5). At both sites, however, sinistral test abundances vary between maxima of >70% and minima of <20% with relatively few intermediate data points (Figures 5b and 5f). At Site 1063 the record is plagued by frequent gaps (Figure 5b) when total counts are <20 (Figure 5c). Distinct percent sinistral test maxima occur during MIS 7a when counts are at a maximum and during MIS 8 when counts are relatively low. Low sinistral test abundances, on the other hand, are accompanied by distinct count maxima during MIS 7c and MIS 7e. At Site 1059, where the record is continuous (at least after ~270 ka), maxima (>70%) occur during MIS 7a and 7d, briefly during MIS 7e, and twice during MIS 8 (Figure 5f). The maxima during MIS 7a, 7d, and 7e are linked to increases in total counts (Figure 5g), but as at Site 1063, the maxima during glacial MIS 8 occur despite low counts.

At both sites, total test counts (Figures 5c and 5g) are high when percent $CaCO_3$ is also high and vice versa (Figures 5d and 5h). At Site 1063, intervals of low *G. truncatulinoides* abundances (<20 tests) correspond to the times when $CaCO_3$ is below 20% (portions of MIS 6, 7a, and 7d). Thus, as during MIS 1–6, dilution and dissolution affect the total counts. The effect is less severe at the shallower Site 1059 where % $CaCO_3$ remains above 20% for most of the time interval (after ~270 ka) leading to generally higher test counts and a continuous percent *G. truncatulinoides* (sinistral) record.

6.3. MIS 9 (Sites 1059 and 1056)

MIS 9, as well as the shouldering parts of glacial intervals MIS 8 and 10, are recorded at gyre margin Sites 1059 and 1056 (Figure 6, upper and lower panels, respectively). As noted above, there is no foraminiferal $\delta^{18}O$ record for this portion of Site 1059, and we rely on the *G. ruber* $\delta^{18}O$ record from Site 1056 for the comparison. In this record, TIV and the substages of MIS 9 are well delineated (Figure 6a or 6e).

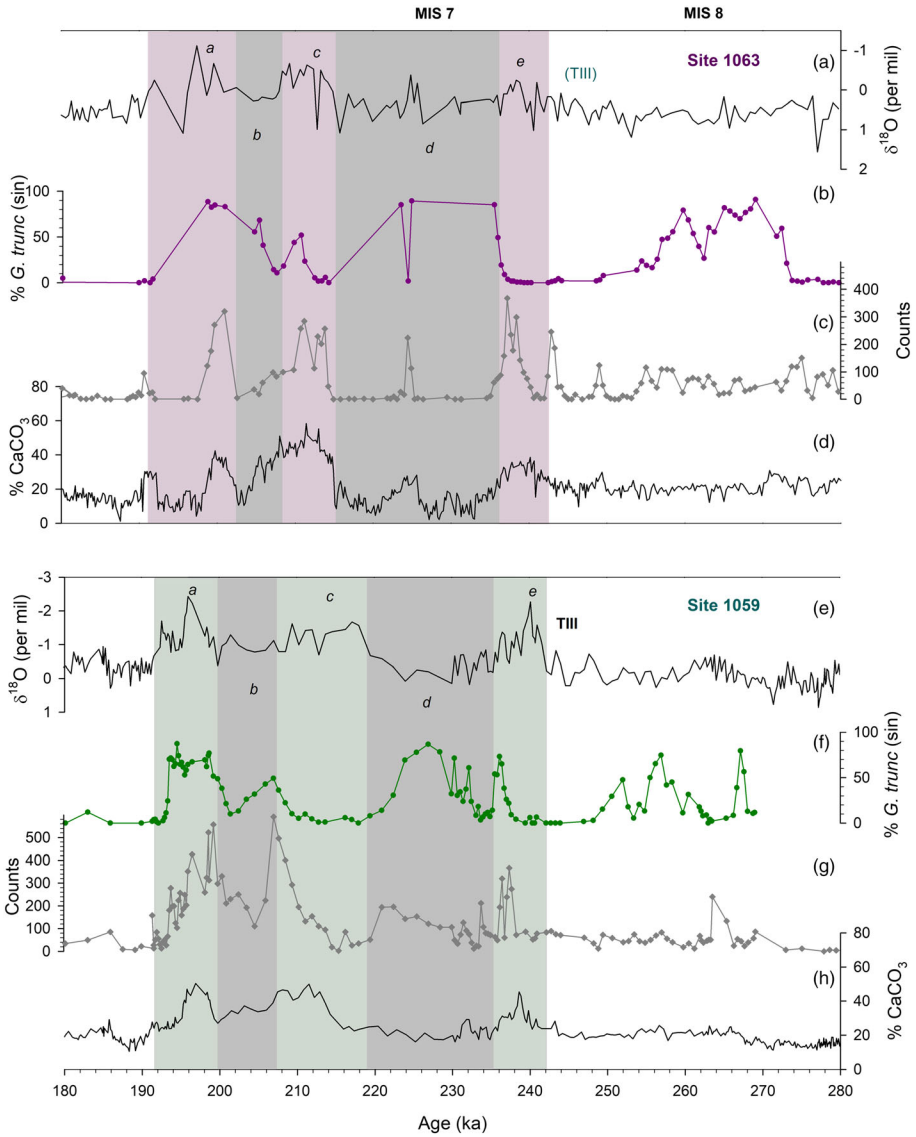

Figure 5. Results from Site 1063 (top panel) and Site 1059 (bottom panel). Shown are (a and e) the sites' planktic foraminiferal δ^{18}O records (Table 1), (b and f) percent *Globorotalia truncatulinoides* (sinistral), (c and g) total *G. truncatulinoides* test counts, and (d and h) percent $CaCO_3$ (Grützner et al., 2002). Marine isotope stages (MIS) are labeled across the top. The color/gray bars identify the marine isotope substages with lettering after Railsback et al. (2015).

Both sites show the same pattern in *G. truncatulinoides* (sinistral) abundances and total test counts. And, as before, sinistral percentages vary between maxima of >70% and minima of <20% with relatively few intermediate data points (Figures 6b and 6f). At both sites, three distinct sinistral test maxima (>70%) occur during MIS 9b, the youngest one crossing into MIS 9a. Sinistral test abundances are low, however, across TIV, MIS 9e through MIS 9c, and during most of MIS 9a. *G. truncatulinoides* (sinistral) abundances are variable during the two glacial intervals, particularly at Site 1056 (Figures 6b and 6f, respectively).

At both sites, total test counts are highest during MIS 9 with some intervals of high counts during MIS 10 (Figures 6c and 6g). Thus, at both sites, the interval of low sinistral percentages between TIV and MIS 9c (and 9a at Site 1056) corresponds to distinct maxima in total counts. During MIS 10, total test counts are also variable, but on the finer scale it appears that the sinistral test maxima tend to be associated with the intervals of lower counts and vice versa.

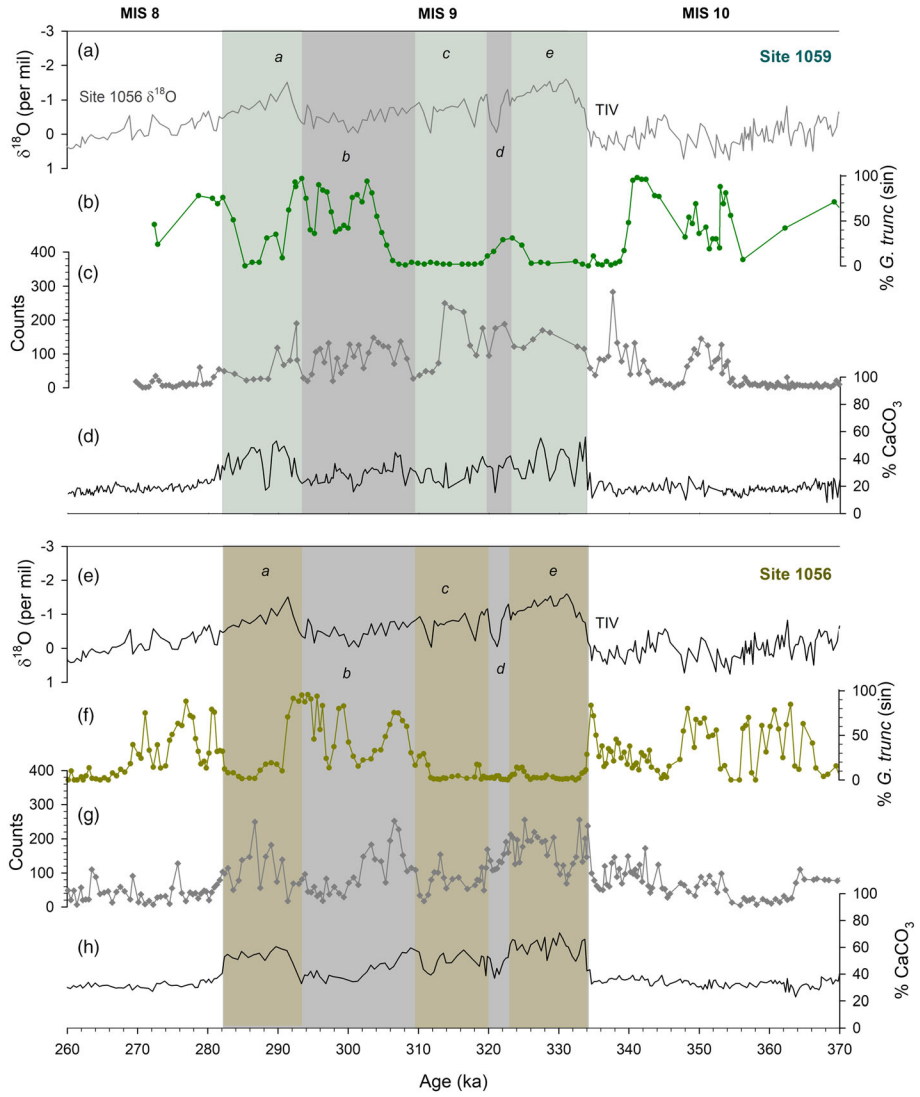

Figure 6. Results from Site 1059 (top panel) and Site 1056 (bottom panel). Shown are (a and e) the sites' planktic foraminiferal $\delta^{18}O$ records (Table 1), (b and f) percent *Globorotalia truncatulinoides* (sinistral), (c and g) total *G. truncatulinoides* test counts, and (d and h) percent $CaCO_3$ (Grützner et al., 2002). Marine isotope stages (MIS) are labeled across the top. The color/gray bars identify the marine isotope substages with lettering after Railsback et al. (2015).

At both sites, variations in total counts largely parallel the percent $CaCO_3$ with relatively high values during MIS 9 (Figures 6d and 6h). During glacial MIS 10, however, the two intervals of relatively high test counts (centered on 340 and 350 ka) occur despite low overall glacial $CaCO_3$ percentages. These increases in test abundances should thus reflect an increase in *G. truncatulinoides* (sinistral) productivity relative to other carbonate producers in the gyre margin.

6.4. MIS 11 (Sites 1056, 1059 and 1058)

Gyre margin Site 1056 and a composite consisting of Sites 1059 and 1058 encompass MIS 11 with shouldering parts of MIS 10 and 12 (Figure 7, upper and lower panels, respectively). As during MIS 9, the $\delta^{18}O$ record from Site 1056 serves as a climate reference for Site 1059, and here, too, it outlines the glacial to interglacial transition (TV) as well as the substages of the ensuing interglacial interval (Figure 7a or 7e). The *G. ruber* $\delta^{18}O$ record from Site 1058 contains high amplitude, millennial-scale variations making it more difficult to identify TV (Weirauch et al., 2008) (Figure 7e).

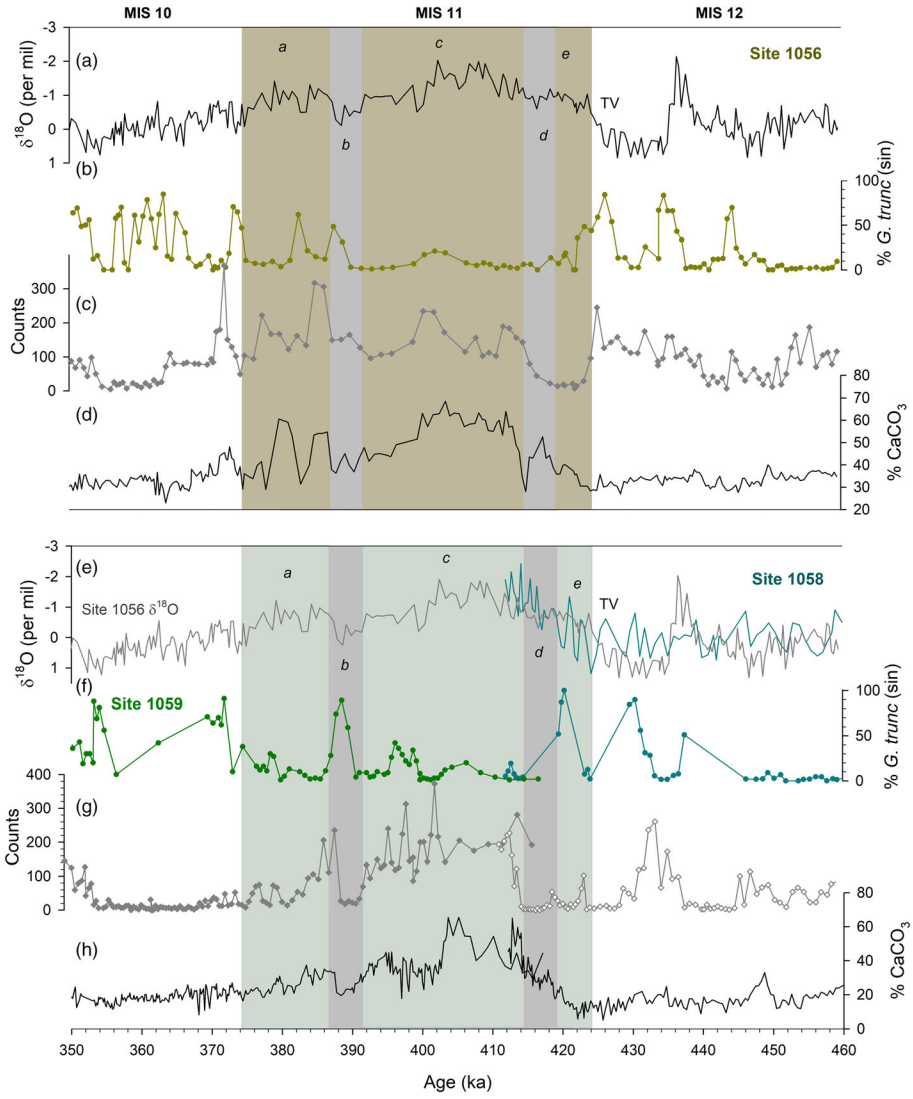

Figure 7. Results from Site 1056 (top panel) and Sites 1059/1058 (bottom panel). Shown are (a and e) the sites' planktic foraminiferal $\delta^{18}O$ records (Table 1), (b and f) percent *Globorotalia truncatulinoides* (sinistral), (c and g) total *G. truncatulinoides* test counts (Site 1059 closed symbols, Site 1058 open symbols), and (d and h) percent $CaCO_3$ (Grützner et al., 2002). Marine isotope stages (MIS) are labeled across the top. The color/gray bars identify the marine isotope substages with lettering after Railsback et al. (2015).

Again, *G. truncatulinoides* (sinistral) maxima and minima vary from >70% to <20% with relatively few intermediate values (Figures 7b and 7f). At both sites, interglacial MIS 11c stands out as a prolonged interval of minimal sinistral test abundances despite high test counts (Figures 7c and 7g). At Site 1059, MIS 11b and MIS 11e stand out as maxima recorded by low total test counts. At both sites, test counts are low during TV and through MIS 11d. In fact, at Site 1056, test counts are lower during MIS 11e than the preceding glacial maximum of MIS 12 (Figure 7c). At Site 1058, on the other hand, test counts tend to be minimal during MIS 12 except for one distinct maximum between ~430 and 436 ka. In the Site1059/1058 composite, there are a number of gaps due to low (<20) total counts during the glacial intervals as well as MIS 11e and 11d (Figure 7g).

Total test counts largely parallel percent $CaCO_3$ with generally high numbers during the majority of the interglacial interval (Figures 7d and 7h). At both sites, count minima occur during TV and MIS 11e during a time of rising percent $CaCO_3$. Conversely, the test count maxima during MIS 12 at Site 1056 occur despite

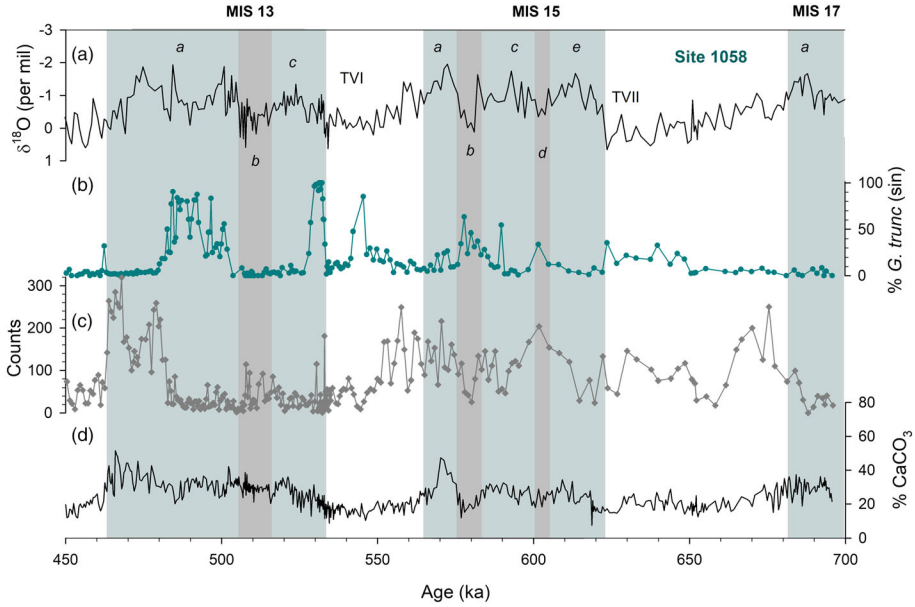

Figure 8. Results from Site 1058. Shown are (a) the site's planktic foraminiferal $\delta^{18}O$ record (Table 1), (b) percent *Globorotalia truncatulinoides* (sinistral), (c) total *G. truncatulinoides* test counts, and (d) percent $CaCO_3$ (Grützner et al., 2002). Marine isotope stages (MIS) are labeled across the top. The color/gray bars identify the marine isotope substages with lettering after Railsback et al. (2015).

low percent $CaCO_3$. Thus, here, too, there is evidence for variations in *G. truncatulinoides* productivity affecting the total counts against background changes in the depositional environment. During the relatively warm interval of MIS 11e, overall *G. truncatulinoides* productivity is low, while during the glacial MIS 12, abundances increase, at times, in relation to other carbonate producers.

6.5. MIS 13–17 (Site 1058)

The *G. ruber* $\delta^{18}O$ record spanning MIS 13–17 outlines glacial to interglacial changes in background climate, and, although it is overprinted by high-frequency, millennial-scale variations, TVI and TVII can be clearly identified (Figure 8a). There is a sustained lack of sinistral tests until MIS 14, and sinistral tests do not dominate (i.e., >50%) for any length of time until MIS 13a (Figure 8b). The new higher resolution record is consistent with the lower resolution data set indicating a long-term disappearance of this morphotype from this and other North Atlantic sites between MIS 21–15 (Kaiser et al., 2019). Test counts are variable between MIS 17 and MIS 15, but decrease during MIS 14 and remain low throughout the majority of MIS 13 until the latter stages of MIS13a.

This interval of time differs from the younger ones in that the total test counts do not parallel the $CaCO_3$ record (Figures 8c and 8d). In comparison to the $CaCO_3$ record, counts are too high during MIS 16, and too low during the majority of MS 13. Only during the younger of the two $\delta^{18}O$ minima defining MIS 13a does the increase in total counts relate to an increase in percent $CaCO_3$.

7. Discussion

7.1. Variations in Percent *G. truncatulinoides* (Sinistral)

In sum, the overall character of glacial to interglacial variations in percent sinistral tests changes through time across three distinct time intervals (Figure 3c). Between MIS 17 and MIS 13, sinistral test maxima increase from near zero to >70% without an apparent glacial to interglacial signal. After MIS 13a and through most of MIS 7, percent sinistral tests vary with maxima >70% and minima <20%. These maxima and minima occur more frequently than the overall glacial to interglacial background conditions. Between MIS 7a and MIS 1, however, there is a distinct association of sinistral test maxima (>70%) with interglacial (MIS 5 and 1) and minima (<10%) with glacial climates (MIS 6, MIS 4, and MIS 2); MIS 3 being an exception at both sites with a maximum during a relatively cold stage. In this regard, the gyre center

Table 2
Summary of Percent Globorotalia truncatulinoides (Sinistral) Abundances Associated With (a) Interglacial Maxima, (b) Warm Substages Defined by Relative $\delta^{18}O$ Minima, and (c) Cold Substages Defined by Relative $\delta^{18}O$ Maxima[a]

	High count		Low count	
MIS	%max	%min	%max	%min
(a)				
1	x, x			
5c	x, x			
5e	x			
7a	x, x			
9c		x, x		
9d		x, x		
9e		x, x		
11c		x, x		
(b)				
5a	x, x	x	x, x	x, x
7c		x, x		x
7e	x	x		x, x
9a	x	x, x		x
11a		x, x		x
11e			x	x, x
13a		x	x	
13c				x
(c)				
5b	x		x	
5d	x, x			x, x
7b				x, x
7d	x	x	x	x
9b	x, x	x, x	x	x
11b		x	x	
11d				x, x
13b				x

[a]Color code corresponds to color code in Figures 4–8: Sites 1063, KNR110–37PC, 1059, 1056, and 1058.

(Site 1063) and gyre margin (KNR 140-37PC and Site 1059) behaved in unison during the last two glacial cycles.

Variations in test counts, on the other hand, do follow an overall glacial (low counts) and interglacial (high counts) pattern closely paralleling the percent $CaCO_3$ record at the sites. This pattern is apparent for the first time during the latter stages of MIS 13a. MIS 12 is the first time that both proxies show some low values at the same time during a glacial interval. Thus, the effects of sediment dilution of the carbonate components by terrigenous materials during glacial intervals starts to dominate the depositional environment of BBOR beginning with MIS 12. Beginning with MIS 11, the pattern of high test counts and high percent $CaCO_3$ during interglacial intervals versus low test counts and low $CaCO_3$ and becomes firmly established.

Within interglacial intervals, there is an association of relatively high test counts with either high (MIS 1, 5e, 5c, and 7a) or low (MIS 9c, 9d, 9e, 11c, and the latter portion of MIS 13a) percent sinistral test abundances at both sites spanning each interval (Table 2a). Low sinistral test percentages in combination with high test counts indicate a high percentage of dextral tests, for which there is no late Holocene analog at the study sites. With few exceptions, these intervals correspond to the "proper" interglacial intervals defined by Past Interglacials Working Group of PAGES (2016) (MIS 1, 5e, 7a–7c, 7e, 9e, 11c). All other marine isotope substages, whether defined by relatively low $\delta^{18}O$ values (such as those labeled "a," "c," and in the case of MIS 11, "e") or high $\delta^{18}O$ values (such as those labeled "b," and "d"), display variable combinations of percent sinistral maxima and minima with test counts and lack a common pattern (Tables 2b and 2c, respectively). Thus, the character of regional subtropical upper water column structure is consistent with the definition of an interglacial interval according to Past Interglacials Working Group of PAGES (2016).

Exceptions to the Past Interglacials Working Group of PAGES (2016) scheme include MIS 5c, 7b, 7c, 7e, and 9c and 9d. With high test counts, MIS 5c, 9c, and 9d look like "true" interglacials (Table 2a), while MIS 7b, with its low percent sinistral tests and low counts is more "glacial-like" (Table 2c). And, neither MIS 7c nor MIS 7e are distinguished by a consistent "interglacial" pattern associated with either maximum or minimum sinistral test abundances and high total test counts (Table 2b).

Glacial intervals, MIS 8, 10, and 12 (and cold MIS 3) also display a number of distinct maxima in sinistral test percentages (e.g., Figure 3c). Counts are generally low because of enhanced dilution with terrigenous sediments, but the presence of these maxima suggests relatively large instabilities in the western boundary current. During MIS 12, when sinistral test maxima at Site 1056 also occur during an interval of high total test counts, three even-spaced maxima (at 424, 434, and 444 ka (Figure 7b)) would be consistent with millennial-scale variations in planktic foraminiferal $\delta^{13}C$ record and faunal assembles prominent during this interval of time (Chaisson et al., 2002).

7.2. Implications on Western Boundary Current Flow Through Time

Between MIS 17 and MIS 13, there is no distinct association among the proxies. Percent *G. truncatulinoides* (sinistral) are low and do not display a consistent pattern. During this time interval, *G. truncatulinoides* counts are not sensitive to sediment dilution and/or dissolution as evidenced by relatively high numbers during glacial MIS 16 and relatively low numbers during interglacials MIS 17a and the majority of MIS 13a. In fact, dilution/dissolution effects may be less important overall during this interval as indicated by lower amplitude variation in the percent $CaCO_3$ record (Figure 8d). Thus, the particular relationship between coiling direction, high total test counts, and high percent $CaCO_3$ during warm intervals first occurs during the end of MIS 13a and becomes firmly established during MIS 11.

The MIS 12 to MIS 11 (TV) transition marks one of the most extreme of the Pleistocene glacial to interglacial transitions, the mid Brunhes event (e.g., Candy & McClymont, 2013; Droxler et al., 2003; Hodell et al., 2000). It appears that the establishment of the coupling between total test counts and percent $CaCO_3$ at BBOR may be related to the climatic changes associated with this event. Of particular pertinence here is that subtropical sea surface temperature and surface ocean salinity changes in the Caribbean have been ascribed to a shift of the Intertropical Convergence Zone toward its modern-day location during interglacial intervals beginning with MIS 11 (Sepulcre et al., 2011). A proxy response (at Sites 1058 and 1056) at the same time as tropical surface ocean hydrographic changes would be consistent with an ocean basin-wide response to the ocean-atmospheric processes governing the mid Brunhes event.

After the mid Brunhes event, during the interglacial maxima of MIS 11c and 9e (and MIS substages 9c, 9d), *G. truncatulinoides* (sinistal) abundances are low while total test abundances are high (Table 2a). Thus, at these times, relatively low sinistral test abundances indicate an increase in the dextral variety. In keeping with the foraminifer's ecology, the decrease in the sinistral, at the expense of an increase in dextral, forms must be associated with a change in the living space toward conditions favoring dextral forms. Such conditions would reflect higher nutrients either associated with a shallower permanent thermocline or due to an influx via surface currents, both more characteristic of the gyre margin (e.g., Ujiié et al., 2010). This could reflect either that the study sites were located landward of the Gulf Stream implying that maximum Gulf Stream flow occurred a bit farther to the southeast than during the late Holocene (e.g., Figure 1). Or, it implies that the westward flowing North Equatorial and northward flowing Antilles Current were shifted toward the northwestern margin of the gyre.

In the former scenario, the inference might indicate a more intensely flowing Gulf Stream drawing away from the coast to conserve angular momentum. This would be supported by observations from the modern ocean of changes in Gulf Stream path being associated with increased gyre circulation (Ezer et al., 2013; Sallenger et al., 2012). These particular studies, however, focus on the mid-Atlantic where the Gulf Stream turns offshore. A faster spinning gyre should also move the region of maximum sea surface height toward the center of the gyre in the latitudes of our study sites; however, we are not aware of modern oceanographic studies that would support this interpretation. We speculate that based on the late Holocene distribution of *G. truncatulinoides* across the Gulf Stream at our study sites (Figure 1), the shift in path may not need to be large. Sites 1054/1055, which show distinctly low sinistral abundances, are only about 180 km away from Sites 1058/1059, which show distinctly high sinistral abundances. This distance is similar to the width of the current system (e.g., Hogg & Johns, 1995) and therefore feasible. Our inference is supported by a study focusing on the MIS 12–11 transition, when westward intensification was invoked to explain millennial-scale changes in Site 1056 planktic foraminiferal stable isotope records and faunal assemblages (Chaisson et al., 2002).

In the latter scenario, high dextral abundances may be associated with changes in the southern extent of the gyre, specifically flow in the North Equatorial Current and the Antilles Current (e.g., Ujiié et al., 2010). We suggest that high dextral forms may reflect an extension of these currents toward the northwestern regions of the gyre. This scenario would imply enhanced westward and northward flow in these currents, respectively, also implying an intensification of subtropical gyre circulation. Under this scenario, intensification of the gyre during MIS 11c, and MIS 9e, (and substages 9c and 9d) could be related to sustained conditions akin to anomalies like the positive phase of the Arctic Oscillation when trade winds and westerly winds strengthen (Justino & Peltier, 2008). Enhanced warm water flow in the North Atlantic Current and a more northerly path of storm tracks causes relative warmth in northern Europe (e.g., Curry & McCartney, 2001). North Atlantic (>56°N) and Arctic Ocean warmth is evident in proxy records spanning MIS 11c (Alonso-Garcia et al., 2011; Bauch et al., 2000; Candy & McClymont, 2013; Cronin et al., 2019). MIS 11c stands out as particularly warm and wet in the Russian Arctic (Lake El'gygytgyn, Melles et al., 2012) and Subarctic (Lake Baikal, Karabanov et al., 2003; Prokopenko et al., 2006). For comparison, proxy records from midlatitudes do not show particular warmth during MIS 11c (e.g., Candy et al., 2010; Candy & McClymont, 2013). MIS 9e is less intense than MIS 11c in the abovementioned lake records, but more intense than the warm peaks of MIS 7, 5, and 1 (Past Interglacials Working Group of PAGES, 2016).

Beginning with MIS 7a, high sinistral test percentages are distinctly related to high total counts during interglacial and low sinistral percentages to low total counts during glacial intervals (e.g., Table 2a). Therefore,

high total *G. truncatulinoides* counts at these times are driven by the increase in the sinistral forms. Thus, the modern-like environment as recorded in core top percentages (Figure 1) becomes established at this time. Site 1063 is deep (~4,600 m), but the lack of *G. truncatulinoides* during TII and the interglacial maximum of MS 5e cannot be explained by dilution or dissolution as the $CaCO_3$ content of the sediments is high at this time (Figure 4g). The different response between the two sites appears to reflect a spatial difference in *G. truncatulinoides* productivity between the margin and center of the gyre, one that disappears during MIS 5d.

Based on foraminiferal $\delta^{18}O$ values, atmospheric CO_2, global sea level, and temperature records, MIS 5e is also viewed as one of the warmer interglacial periods, although it does not stand out as such in the high northern latitude lake records (e.g., Past Interglacials Working Group of PAGES, 2016). That observation would be consistent with our *G. truncatulinoides* records that show a different response during this interval of time. Dominance of sinistral forms during TII and MIS 5e (gyre margin only) as well as TI and MIS 1 (both sites) might indicate more localized changes in the western boundary current and the subtropical gyre.

The increase in sinistral test abundances during TI (both sites) and TII (KNR110–37 PC) is consistent with a recovery from a compressed subtropical gyre after the glacial extremes. For the LGM, a compressed subtropical gyre is supported by planktic foraminiferal $\delta^{18}O$ records (Billups & Schrag, 2000) and low planktic foraminiferal abundances (Pflaumann et al., 2003). Our data support that as climate warmed during the deglaciation, subtropical atmospheric circulation shifted toward modern conditions causing downwelling in the center of the gyre reestablishing *G. truncatulinoides*, and in particular its sinistral form, in the center of the gyre (Site 1063) and near its western boundary current (KNR140-37PC; Billups et al., 2016). This scenario is consistent with reconstructions of thermocline conditions for TII and interglacial MIS 5e based on stable isotope and Mg/Ca ratios in *G. truncatulinoides* (Bahr et al., 2013).

Regardless of the specific mechanism, the prolonged percent sinistral minima during MIS 11c and MIS 9e–9c as well as the prolonged maxima during MIS 5e–5c and MIS 1 suggest that the western boundary current remained stable in its position during the entire duration of these warm periods. On the other hand, the current was comparatively less stable during cold intervals when incursions of sinistral tests to >70% of the assemble suggest a landward expansion of the deep subtropical warm pool. This is particularly evident during MIS 3 and at relatively high frequencies during glacial MIS 8, 10, and 12.

8. Summary and Conclusions

G. truncatulinoides in the northwestern subtropical Atlantic provide a sensitive proxy for the relative stability and intensity of the western boundary current. The association between total counts and coiling direction and percent $CaCO_3$ is first evident during the later stages of MIS 13a and becomes firmly established with MIS 11 suggesting a response to changes in ocean–atmosphere processes related to the mid Brunhes event. Thereafter, total counts are consistently high during those interglacial intervals that are deemed proper interglacial maxima based on the definition of Past Interglacials Working Group of PAGES (2016). During these times there are distinct sinistral test maxima (MIS 1, 5e, and 7a) or minima (MIS 9e and 11c), the latter reflecting dominance of the dextral forms. During interglacial maxima of MIS 11c and MIS 9e, dominance of dextral forms suggests enhanced gyre circulation either drawing the northwestern margin centerward or a northwestern more extend of the southern gyre boundary as perhaps related to conditions akin to a positive phase of the Arctic Oscillation. Regardless of the mechanisms, sinistral test minima being prolonged during these times suggest that the western boundary current remained relatively stable during these interglacial maxima. Dominance of sinistral forms during TII (gyre margin) and TI (both sites) and the ensuing interglacial maxima of MIS 5e (gyre margin only) and MIS 1 (both sites) suggest recovery of the gyre after the glacial maxima toward modern conditions. Our results would also suggest that interglacial maxima MIS 11c and 9e are characterized by more intense gyre flow than MIS 5e and 1. However, the prolonged sinistral test maxima during MIS 5 and 1 indicate that the position of the western boundary current also remained relatively stable during these more recent warm intervals.

In conclusion, our results have implications on the relationship between gyre flow and regional mid-Atlantic sea level. Specifically, our results suggest that without anthropogenic forcing, intervals of peak warmth are associated with more intense flow in the western boundary current, which, by extension, would counteract a portion of the glacioeustatic sea level rise. At the same time, the position of the western boundary current

appears to be relatively stable during these warm intervals, at least on the 500–2,000 year time resolution of this study.

Data Availability Statement

All data are archived electronically at the NOAA World Data Center-A for Paleoclimate (https://www.ncdc.noaa.gov/paleo/study/30952).

Acknowledgments
We thank the Editors for their time handling this manuscript. We are especially grateful to two anonymous reviewers and André Bahr who have provided thoughtful and constructive feedback on an earlier version of this manuscript. We thank Justin Guider and Randy Feris for helping with *G. truncatulinoides* coiling direction counts. NSF provided support via the site REU award to the School of Marine Science and Policy of the University of Delaware (grant number 1757840) in the context of which *G. truncatulinoides* coiling was established for Site 1056 (Josie Chiarello). Maoli Vizcaíno thanks the University of Delaware for a Graduate Fellowship. This research used samples provided by the Ocean Drilling Program (ODP). ODP is sponsored by the U.S. National Science Foundation (NSF) and participating countries under the management of the Joint Oceanographic Institutions, Inc.

References

Alonso-Garcia, M., Sierro, F. J., & Flores, J. A. (2011). Arctic front shifts in the subpolar North Atlantic during the mid-Pleistocene (800–400 ka) and their implications for ocean circulation. *Palaeogeography, Palaeoclimatology, Palaeoecology*, *311*, 268–280. https://doi.org/10.1016/j.palaeo.2011.09.004

Bahr, A., Nürnberg, D., Karas, C., & Grützner, J. (2013). Millennial-scale versus long-term dynamics in the surface and subsurface of the western North Atlantic subtropical gyre during Marine Isotope Stage 5. *Global and Planetary Change*, *111*, 77–87.

Bauch, H. A., Erlenkeuser, H., Jung, S. J. A., & Thiede, J. (2000). Surface and deep water changes in the subpolar North Atlantic during Termination II and the Last Interglaciation. *Paleoceanography*, *15*(1), 76–84. https://doi.org/10.1029/1998PA000343

Billups, K., Chaisson, W., Worsnopp, M., & Thunell, R. (2004). Millennial-scale fluctuations in subtropical Northwestern Atlantic surface ocean thermal stratification. *Paleoceanography*, *19*, PA2017. https://doi.org/10.1029/2003PA000990

Billups, K., Hudson, C., Kunz, H., & Rew, I. (2016). Exploring Globorotalia truncatulinoides coiling ratios as a proxy for subtropical gyre dynamics in the northern Atlantic Ocean during the late Pleistocene ice ages. *Paleoceanography*, *31*, 553–563. https://doi.org/10.1002/2016PA002927

Billups, K., Rabideaux, N., & Stoffel, J. (2011). Suborbital-scale surface and deep water records in the subtropical North Atlantic: Implications on thermohaline overturn. *Quaternary Science Reviews*, *30*, 2976–2987.

Billups, K., & Scheinwald, A. (2014). Origin of millennial-scale climate signals in the subtropical North Atlantic. *Paleoceanography*, *29*, 612–627. https://doi.org/10.1002/2014PA002641

Billups, K., & Schrag, D. P. (2000). Surface Ocean density gradients during the Last Glacial Maximum. *Paleoceanography*, *15*, 110–123.

Candy, I., Coope, G. R., Lee, J. R., Parfitt, S. A., Preece, R. C., Rose, J., & Schreve, D. C. (2010). Pronounced warmth during early middle Pleistocene interglacials:Investigating the mid-Brunhes event in the British terrestrial sequence. *Earth-Science Reviews*, *103*, 183–196.

Candy, I., & McClymont, E. L. (2013). Interglacial intensity in the North Atlantic over the last 800,000 years: Investigating the complexity of the mid-Brunhes event. *Journal of Quaternary Sciences*, *23*, 343–348.

Chaisson, W. P., Poli, M.-S., & Thunell, R. C. (2002). Gulf stream and western boundary undercurrent variations during MIS 10-12 at site 1056, Blake-Bahama outer ridge. *Marine Geology*, *189*, 79–105.

Channell, J. E. T., Hodell, D. A., & Curtis, J. H. (2012). ODP Site 1063 (Bermuda rise) revisited: Oxygen isotopes, excursions and paleointensity in the Brunhes Chron. *Geochemistry, Geophysics, Geosystems*, *13*, Q02001. https://doi.org/10.1029/2011GC003897

Cronin, T. M., Keller, K. J., Farmer, J. R., Schaller, M. F., O'Regan, M., & Poirier, R. (2019). Interglacial paleoclimate in the Arctic. *Paleoceanography and Paleoclimatology*, *34*(12), 1959–1979. https://doi.org/10.1029/2019PA003708

Curry, R. G., & McCartney, M. S. (2001). Ocean gyre circulation changes associated with the North Atlantic oscillation. *Journal of Physical Oceanography*, *31*, 3374–3400.

De Vargas, C., Renaud, S., Hilbrecht, H., & Pawlowski, J. (2001). Pleistocene adaptive radiation in *Globorotalia truncatulinoides*: Genetic, morphologic, and environmental evidence. *Paleobiology*, *27*, 104–125.

Deuser, W., & Ross, E. H. (1989). Seasonally abundant planktonic foraminifera of the Sargasso Sea: Succession, deep-water fluxes, isotopic compositions, and paleoceanographic implications. *The Journal of Foraminiferal Research*, *19*(4), 268–293.

Droxler, A. W., Alley, R. B., Howard, W. R., Poore, R. Z., & Burckle, L. H. (2003). Unique and exceptionally long interglacial marine isotope stage 11: Window into earth warm future climate. In *Geophysical Monograph Series* (Vol. 137, pp. 1–14). Hoboken, NJ: Blackwell Publishing Ltd. https://doi.org/10.1029/137GM01

Ericson, D., Wollin, G., & Wollin, J. (1954). Coiling direction of *Globorotalia truncatulinoides* in deep-sea cores. *Deep Sea Research*, *2*, 152–158.

Ezer, T., Atkinson, L. P., Corlett, W. B., & Blanco, J. L. (2013). Gulf Stream's induced sea level rise and variability along the U.S. mid-Atlantic coast. *Journal of Geophysical Research: Oceans*, *118*, 685–697. https://doi.org/10.1002/jgrc.20091

Feldmeijer, W., Metcalfe, B., Brummer, G., & Ganssen, G. (2014). Reconstructing the depth of the permanent thermocline through the morphology and geochemistry of the deep dwelling planktonic foraminifer *Globorotalia truncatulinoides*. *Paleoceanography*, *30*, 1–22. https://doi.org/10.1002/2014PA002687

Grützner, J., Giosan, L., Franz, S. O., Tiedemann, R., Cortijo, E., Chaisson, W. P., et al. (2002). Astronomical age models for Pleistocene drift sediments from the western North Atlantic (ODP sites 1056 to 1063). *Marine Geology*, *189*, 5–23.

Hagen, S., & Keigwin, L. D. (2002). Sea-surface temperature variability and deep water reorganization in the subtropical North Atlantic during Isotope Stage 2–4. *Marine Geology*, *189*, 145–162.

Hemleben, C., Spindler, M., Breitinger, I., & Deuser, W. G. (1985). Field and laboratory studies on the ontogeny and ecology of some globorotaliid species from the Sargasso Sea off Bermuda. *Journal of Foraminiferal Research*, *15*, 254–272.

Herman, Y. (1972). *Globorotalia truncatulinoides*: A palaeo-oceanographic indicator. *Nature*, *238*(5364), 394–396. https://doi.org/10.1038/238394a0

Hodell, D. A., Charles, C. D., & Ninnemann, U. S. (2000). Comparison of interglacial stages in the South Atlantic sector of the southern ocean for the past 450 kyr: Implifications for marine isotope stage (MIS) 11. *Global and Planetary Change*, *24*(1), 7–26.

Hogg, N. G., & Johns, W. E. (1995). Western boundary currents. *Reviews of Geophysics*, *33*(suppl), 1311–1334.

Justino, F., & Peltier, W. R. (2008). Climate anomalies induced by the Arctic and Antarctic oscillations glacial maximum and present day perspectives. *Journal of Climate*, *21*, 459–475. https://doi.org/10.1175/2007CLI1703.1

Kaiser, E., Caldwell, A., & Billups, K. (2019). Subtropical gyre geometry during the mid-Pleistocene climate transition. *Paleoceanography and Paleoclimatology*, *34*(4), 658–671. https://doi.org/10.1029/2018PA003502

Karabanov, E. B., Prokopenko, A. A., Williams, D. F., Khursevich, G. K., Kuzmin, M. I., Bezrukova, E. V., & Gvozdkov, A. (2003). High-resolution MIS 11 record from the continental sedimentary archive of Lake Baikal, Siberia. In A. Droxler, R. Poore, &

L. Burckle (Eds.), *Earth's climate and orbital eccentricity: The marine isotope Stage 11* (pp. 223–230). Washington: American Geophysical Union.
Keigwin, L. D., Rio, D., Acton, G. D., et al. (1998). *Proceedings of the Ocean Drilling Program, Initial Reports* (Vol. 172). College Station, TX. https://doi.org/10.2973/odp.proc.ir.172.1998
Kucera, M., Rosell-Melé, A., Schneider, R., Waelbroeck, C., & Weinelt, M. (2005). Multiproxy approach for the reconstruction of the glacial ocean surface (MARGO). *Quaternary Science Reviews*, *24*(7–9), 813–819. https://doi.org/10.1016/j.quascirev.2004.07.017
LeGrande, A. N., & Lynch-Stieglitz, J. (2007). Surface currents in the western North Atlantic during the Last Glacial Maximum. *Geochemistry, Geophysics, Geosystems*, *8*(1–8). https://doi.org/10.1029/2006gc001371
Lisiecki, L. E., & Raymo, M. E. (2005). A Pliocene-Pleistocene stack of 57 globally distributed benthic $\delta^{18}O$ records. *Paleoceanography*, *20*, PA1003. https://doi.org/10.1029/2004PA001071
Locarnini, R. A., Mishonov, A. V., Antonov, J. I., Boyer, T. P., Garcia, H. E., Baranova, O. K., et al. (2010). In S. Levitus (Ed.), *World Ocean Atlas 2009, Volume 1: Temperature*, *NOAA Atlas NESDIS 68* (pp. 1–184). Washington, DC: U.S. Government Printing Office.
Lynch-Stieglitz, J., Curry, W. B., & Slowey, N. (1999). Weaker Gulf Stream in the Florida Straits during the Last Glacial Maximum. *Nature*, *402*(6762), 644–648. https://doi.org/10.1038/45204
Matsumoto, K., & Lynch-Stieglitz, J. (2003). Persistence of gulf stream separation during the last glacial period: Implications for current separation theories. *Journal of Geophysical Research*, *108*, 3174. https://doi.org/10.1029/2001JC000861
Melles, M., Brigham-Grette, J., Minyuk, P. S., Nowaczyk, N. R., Wennrich, V., DeConto, R., et al. (2012). 2.8 million years of Arctic climate change from Lake El'gygytgyn, NE Russia. *Science*, *337*(6092), 315–320. https://doi.org/10.1126/science.1222135
Past Interglacials Working Group of PAGES (2016). Interglacials of the last 800,000 years. *Reviews of Geophysics*, *54*, 162–219. https://doi.org/10.1002/2015RG000482
Pflaumann, U., Sarnthein, M., Chapman, M., d'Abreu, L., Funnell, B., Huels, M., et al. (2003). Glacial North Atlantic: Sea surface conditions reconstructed by GLAMAP 2000. *PANGAEA*, *18*(3). https://doi.org/10.1029/2002PA000774
Prokopenko, A. A., Hinnov, L. A., Williams, D. F., & Kuzmin, M. I. (2006). Orbital forcing of continental climate during the Pleistocene: A complete astronomically tuned climatic record from Lake Baikal, SE Siberia. *Quaternary Science Reviews*, *25*(23–24), 3431–3457. https://doi.org/10.1016/j.quascirev.2006.10.002
Quillévéré, F., Morard, R., Escarguel, G., Douady, C. J., Ujiié, Y., de Garidel-Thoron, T., & de Vargas, C. (2013). Global scale same-specimen morpho-genetic analysis of *Truncorotalia truncatulinoides*: A perspective on the morphological species concept in planktonic foraminifera. *Palaeogeography, Palaeoclimatology, Palaeoecology*, *391*, 2–12.
Railsback, L. B., Gibbard, P. L., Head, M. J., Voarintsoa, N. R. G., & Toucanne, S. (2015). An optimized scheme of lettered marine isotope substages for the last 1.0 million years, and the climatostratigraphic nature of isotope stages and substages. *Quaternary Science Reviews*, *111*, 94–106. https://doi.org/10.1016/j.quascirev.2015.01.012
Rahmstorf, S. (2002). Ocean circulation and climate during the past 120,000 years. *Nature*, *419*(6903), 207–214. https://doi.org/10.1038/nature01090
Sallenger, A. H., Jr., Doran, K. S., & Howd, P. A. (2012). Hotspot of accelerated sea-level rise on the Atlantic coast of North America. *Nature Climate Change*, *2*(12), 884–888. https://doi.org/10.1038/nclimate1597
Sepulcre, S., Vidal, L., Tachikawa, K., Rostek, F., & Bard, E. (2011). Sea-surface salinity variations in the northern Caribbean Sea across the mid-Pleistocene transition. *Climate of the Past*, *7*, 75–90. https://doi.org/10.5194/cp-7-75-2011
Thiede, J. (1971). Variations in coiling ratio of Holocene planktonic foraminifera. *Deep Sea Research*, *18*, 823–831.
Ujiié, Y., de Garidel-Thoron, T., Watanabe, S., Wiebe, P., & de Vargas, C. (2010). Coiling dimorphism within a genetic type of the planktonic foraminifer *Globorotalia truncatulinoides*. *Marine Micropaleontology*, *77*, 145–153.
Ujiié, Y., & Lipps, J. H. (2009). Cryptic diversity in planktonic foraminifera in the northwestern Pacific Ocean. *Journal of Foraminiferal Research*, *39*(3), 145–154.
Weirauch, D., Billups, K., & Martin, P. (2008). Evolution of millennial-scale climate variability during the mid Pleistocene. *Paleoceanography*, *23*, PA3216. https://doi.org/10.1029/2007PA001584